京都大学防災研究所年報 第 53 号 B 平成 22 年 6 月
Annuals of Disas. Prev. Res. Inst., Kyoto Univ., No. 53 B, 2010

Bank Erosion Model along Banks Composed of both Cohesive and Non-Cohesive Material Layers

Hiroshi TAKEBAYASHI, Masaharu FUJITA and Puji HARSANTO

Synopsis

It is often observed banks which have the alternate layers between cohesive sediment layers and non-cohesive sediment layers in natural rivers (ex. the Sesayap River, East Kalimantan Province, Indonesia and so on). In this study, mathematical model of bank erosion process for banks with both the cohesive and the non-cohesive layers is developed. Furthermore, the model is installed into the horizontal two dimensional channel deformation model. The governing equations of the channel deformation model are written in boundary fitted moving general coordinate system. The results indicate that the horizontal shift speed of banks changes with time very much. When the bottom layer is not exposed to the flow, the speed of bank erosion is very slow. However, when bed near the bank is eroded with time and bottom layer starts to be exposed to flow, the bank erosion rate increases rapidly and it is considered that a severe disaster is caused. The calculated horizontal shape of bank lines is not so smooth and local curvature of bank lines becomes small.

Keywords: bank erosion, cohesive material, numerical analysis, moving general coordinate system

1. Introduction

It is often observed banks which have the alternate layers between cohesive sediment layers and non-cohesive sediment layers in natural rivers. The top sediment layer of banks in the Sesayap River, East Kalimantan Province, Indonesia has cohesive characteristics. On the other hand, the bottom layer of the banks and the bed material are composed of coarser material and does not have cohesive characteristics. The Kushiro River, Hokkaido, Japan also has two kinds of layers in banks. The top sediment layer is made of peat and includes vegetable fibers. Hence the erosion rate of the sediment is very slow. However, the bottom layer of banks and the bed material are composed of sand and do not have cohesive characteristics.

In this study, mathematical model of bank erosion process for banks with both the cohesive and non-cohesive layers is developed. In the model, it is assumed that the top layer has cohesive characteristics and both bottom layer and bed has no cohesive characteristics as we can often observed in rivers all over the world. Hence the bottom layer in banks is eroded by the landslide due to the bed degradation near the bank. The top layer in banks is eroded directly by the flow and indirectly by bank failure due to the erosion of bottom layer. Furthermore, the model is installed into the horizontal two dimensional channel deformation model and channel deformation process is simulated. The governing equations of the channel deformation model are written in boundary fitted moving general coordinate system.

2. Example of natural river bank composed of both cohesive and non-cohesive materials

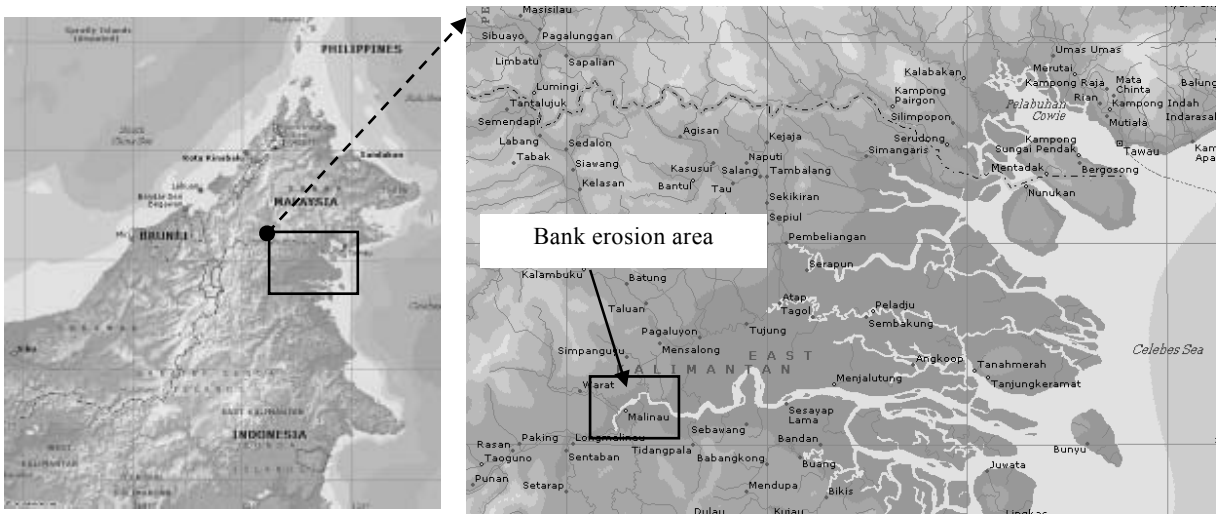

Figure 1 Location of Malinau at Sesayap River

Figure 2 River bank failure and flood at Seluwing Malinau

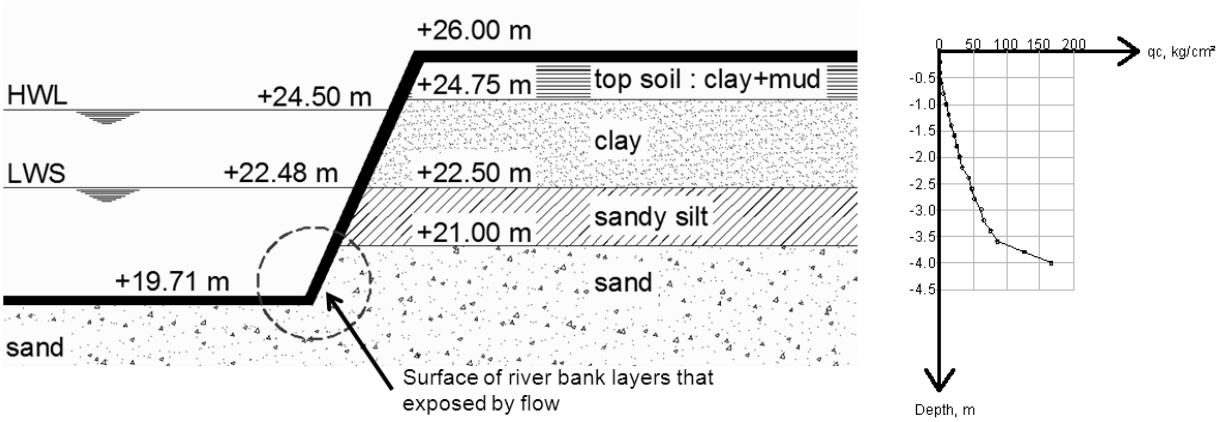

Figure 3 Cross section and water surface elevation at river bend

Sesayap River is located at East Kalimantan Indonesia. The river is 279 km long and the catchment has an area of about 18158 km^2. Sesayap River works as a navigation channel which conducts between Malinau, Nunukan and Tarakan. The estuary of Sesayap River is located at Celebes Sea around 70 km from Malinau.

The surveyed area is Seluwing bend on the river reach that located at Malinau (Figure 1). The river bed material is composed of coarse gravel, cobbles and sand. Riverbank around these reach was collapsed on April and September 2008. They give huge damages on the road structure (Figure 2). On November 2008, flood was occurred with 30 cm depth on the floodplan (Figure 2).

The surveyed area is influenced by tide from Celebes Sea that creates a diurnal water level fluctuation. However, the flow is always on the

downstream direction. Fluctuation of water level is around 1-3 meters. The higher water level is around 24.50 m and 22.50 m at the lower condition (Figure 3). The fluctuations of water level make wet condition on the bank surface. At the middle of the channel, there is sediment deposition whose bed level is 23.00m. Elevation at the toe of the riverbank is 19.71 m and at the top of bank is 25.00 m.

River bed elevation is measured using Garmin GPS-MAP 178 Sounder for 12 km long. Sediment data is obtained at 2 locations in the riverbank by cone penetration test and hand boring. The results from soil test indicate that the bank consist of finer grain size, which lie on four layers. The first top layer is composed of soil, which is 1 m thickness. The second layer has 1.75 m thickness. These soil layers have specific gravity, angle of internal friction and cohesion, respectively, 2.6, 10°, 9 kN/m^2. The third layer is sandy silt, which has specific gravity, angle of internal friction and cohesion, respectively, 2.65, 32.5°, 5 kN/m^2. The bottom layer is composed of sand.

3. Numerical analysis method

3 1. Governing equations

Computation of surface flow is performed using the governing equation of the horizontal two dimensional flow averaged with depth. The conservation of mass, i.e., inflow and outflow of mass by seepage flow, is taken into consideration as shown in the following equation [10].

$$\Lambda\frac{\partial}{\partial t}\left(\frac{z}{J}\right)+\frac{\partial}{\partial\xi}\left(\left(\frac{\partial\xi}{\partial t}+U\right)\frac{h}{J}\right)+\frac{\partial}{\partial\eta}\left(\left(\frac{\partial\eta}{\partial t}+V\right)\frac{h}{J}\right)+\frac{\partial}{\partial\xi}\left(\left(\frac{\partial\xi}{\partial t}+U_g\right)\frac{h_g}{J}\right)+\frac{\partial}{\partial\eta}\left(\left(\frac{\partial\eta}{\partial t}+V_g\right)\frac{h_g}{J}\right)=0 \quad (1)$$

where, ξ and η are the coordinates along the longitudinal and the transverse directions in generalized coordinate system, respectively. x and y are the coordinates in Cartesian coordinate system, respectively. t is the time, z is the water surface level. Surface flow depth is represented as h, seepage flow depth is h_g. U and V represent the contravariant depth averaged flow velocity on bed along ξ and η coordinates, respectively. U_g and V_g represent the contravariant depth averaged seepage flow velocity along ξ and η coordinates, respectively. Momentum equations of surface water are as follows.

$$\begin{aligned}
&\frac{\partial}{\partial t}\left(\frac{hU}{J}\right)+\frac{\partial}{\partial\xi}\left(U_t\frac{hU}{J}\right)+\frac{\partial}{\partial\eta}\left(V_t\frac{hU}{J}\right)\\
&-\frac{hu}{J}\left(\frac{\partial}{\partial t}\left(\frac{\partial\xi}{\partial x}\right)+U_t\frac{\partial}{\partial\xi}\left(\frac{\partial\xi}{\partial x}\right)+V_t\frac{\partial}{\partial\eta}\left(\frac{\partial\xi}{\partial x}\right)\right)\\
&-\frac{hv}{J}\left(\frac{\partial}{\partial t}\left(\frac{\partial\xi}{\partial y}\right)+U_t\frac{\partial}{\partial\xi}\left(\frac{\partial\xi}{\partial y}\right)+V_t\frac{\partial}{\partial\eta}\left(\frac{\partial\xi}{\partial y}\right)\right)\\
&=-gh\left(\frac{1}{J}\left(\left(\frac{\partial\xi}{\partial x}\right)^2+\left(\frac{\partial\xi}{\partial y}\right)^2\right)\frac{\partial z_s}{\partial\xi}\right)\\
&\quad-gh\left(\frac{1}{J}\left(\frac{\partial\xi}{\partial x}\frac{\partial\eta}{\partial x}+\frac{\partial\xi}{\partial y}\frac{\partial\eta}{\partial y}\right)\frac{\partial z_s}{\partial\eta}\right)-\frac{\tau_{b\xi}}{\rho J}\\
&\quad+\frac{1}{J}\left(\frac{\partial\xi}{\partial x}\right)^2\frac{\partial}{\partial\xi}\left(h\sigma_{xx}\right)+\frac{1}{J}\frac{\partial\xi}{\partial x}\frac{\partial\eta}{\partial x}\frac{\partial}{\partial\eta}\left(h\sigma_{xx}\right)\\
&\quad+\frac{1}{J}\frac{\partial\xi}{\partial y}\frac{\partial\eta}{\partial x}\frac{\partial}{\partial\eta}\left(h\tau_{yx}\right)+\frac{1}{J}\frac{\partial\xi}{\partial y}\frac{\partial\xi}{\partial x}\frac{\partial}{\partial\xi}\left(h\tau_{yx}\right)\\
&\quad+\frac{1}{J}\frac{\partial\xi}{\partial x}\frac{\partial\eta}{\partial y}\frac{\partial}{\partial\eta}\left(h\tau_{xy}\right)+\frac{1}{J}\frac{\partial\xi}{\partial x}\frac{\partial\xi}{\partial y}\frac{\partial}{\partial\xi}\left(h\tau_{xy}\right)\\
&\quad+\frac{1}{J}\left(\frac{\partial\xi}{\partial y}\right)^2\frac{\partial}{\partial\xi}\left(h\sigma_{yy}\right)+\frac{1}{J}\frac{\partial\xi}{\partial y}\frac{\partial\eta}{\partial y}\frac{\partial}{\partial\eta}\left(h\sigma_{yy}\right)
\end{aligned} \quad (2)$$

$$\begin{aligned}
&\frac{\partial}{\partial t}\left(\frac{hV}{J}\right)+\frac{\partial}{\partial\xi}\left(U_t\frac{hV}{J}\right)+\frac{\partial}{\partial\eta}\left(V_t\frac{hV}{J}\right)\\
&-\frac{hu}{J}\left(\frac{\partial}{\partial t}\left(\frac{\partial\eta}{\partial x}\right)+U_t\frac{\partial}{\partial\xi}\left(\frac{\partial\eta}{\partial x}\right)+V_t\frac{\partial}{\partial\eta}\left(\frac{\partial\eta}{\partial x}\right)\right)\\
&-\frac{hv}{J}\left(\frac{\partial}{\partial t}\left(\frac{\partial\eta}{\partial y}\right)+U_t\frac{\partial}{\partial\xi}\left(\frac{\partial\eta}{\partial y}\right)+V_t\frac{\partial}{\partial\eta}\left(\frac{\partial\eta}{\partial y}\right)\right)\\
&=-gh\left(\frac{1}{J}\left(\frac{\partial\xi}{\partial x}\frac{\partial\eta}{\partial x}+\frac{\partial\xi}{\partial y}\frac{\partial\eta}{\partial y}\right)\frac{\partial z_s}{\partial\xi}\right)\\
&\quad-gh\left(\frac{1}{J}\left(\left(\frac{\partial\eta}{\partial x}\right)^2+\left(\frac{\partial\eta}{\partial y}\right)^2\right)\frac{\partial z_s}{\partial\eta}\right)-\frac{\tau_{b\eta}}{\rho J}\\
&\quad+\frac{1}{J}\frac{\partial\eta}{\partial x}\frac{\partial\xi}{\partial x}\frac{\partial}{\partial\xi}\left(h\sigma_{xx}\right)+\frac{1}{J}\left(\frac{\partial\eta}{\partial x}\right)^2\frac{\partial}{\partial\eta}\left(h\sigma_{xx}\right)\\
&\quad+\frac{1}{J}\frac{\partial\eta}{\partial y}\frac{\partial\xi}{\partial x}\frac{\partial}{\partial\xi}\left(h\tau_{yx}\right)+\frac{1}{J}\frac{\partial\eta}{\partial y}\frac{\partial\eta}{\partial x}\frac{\partial}{\partial\eta}\left(h\tau_{yx}\right)\\
&\quad+\frac{1}{J}\frac{\partial\eta}{\partial x}\frac{\partial\xi}{\partial y}\frac{\partial}{\partial\xi}\left(h\tau_{xy}\right)+\frac{1}{J}\frac{\partial\eta}{\partial x}\frac{\partial\eta}{\partial y}\frac{\partial}{\partial\eta}\left(h\tau_{xy}\right)\\
&\quad+\frac{1}{J}\frac{\partial\eta}{\partial y}\frac{\partial\xi}{\partial y}\frac{\partial}{\partial\xi}\left(h\sigma_{yy}\right)+\frac{1}{J}\left(\frac{\partial\eta}{\partial y}\right)^2\frac{\partial}{\partial\eta}\left(h\sigma_{yy}\right)
\end{aligned} \quad (3)$$

where $U_t=\frac{\partial\xi}{\partial t}+U$, $V_t=\frac{\partial\eta}{\partial t}+V$, g is the gravity, $\rho$is the water density. Λ is a parameter related to the

porosity in the soil, wherein $\Lambda = 1$ as $z \geqq z_b$, and $\Lambda = \lambda$ as $z < z_b$, where z_b is the bed level and λ is the porosity in the soil. Seepage flow is assumed as horizontal two-dimensional saturation flow. $\tau_{b\xi}$ and $\tau_{b\eta}$ represent the contravariant shear stress along ξ and η coordinates, respectively. u_* is the friction velocity as follows.

$$u_*^2 = \frac{u^2 + v^2}{\left(6 + 2.5 \ln \frac{h}{k_s}\right)^2} \tag{4}$$

where, k_s is the roughness height. u_b and v_b represent velocity near the bed surface along x and y coordinates, respectively. Velocities near the bed are evaluated using curvature radius of streamlines as follows.

$$u_b = u_{bs} \cos\alpha_s - v_{bs} \sin\alpha_s \tag{5}$$

$$v_b = u_{bs} \sin\alpha_s + v_{bs} \cos\alpha_s \tag{6}$$

$$u_{bs} = 8.5 u_* \tag{7}$$

$$v_{bs} = -N_* \frac{h}{r} u_{bs} \tag{8}$$

where, $\alpha_s = \arctan(v/u)$, N_* is 7.0 [4] and r is the curvature radius of stream lines obtained by depth integrated velocity field as follows [9].

$$\frac{1}{r} = \frac{1}{\left(u^2 + v^2\right)^{3/2}} \left\{ u\left(u\frac{\partial v}{\partial x} - v\frac{\partial u}{\partial x} \right) + v\left(u\frac{\partial v}{\partial y} - v\frac{\partial u}{\partial y} \right) \right\} \tag{9}$$

σ_{xx}, σ_{yy}, τ_{xy} and τ_{yx} are turbulence stresses, κ is the Karman constant. When the water depth of surface flow becomes less than the mean diameter of the bed material, the surface flow is computed only in consideration of the pressure term and bed shear stress term in the momentum equation of surface flow [7]. Grain size distribution is evaluated using the sediment transport multilayer model as follows [11]:

$$\frac{\partial}{\partial t}\left(\frac{c_b E_b f_{bk}}{J} \right) + (1-\lambda) F_{bk} \frac{\partial}{\partial t}\left(\frac{z_b}{J} \right) + \frac{\partial}{\partial \xi}\left(\frac{\partial \xi}{\partial t} \frac{c_b E_b f_{bk} r_b}{J} + \frac{q_{b\xi k}}{J} \right) \frac{\partial}{\partial \eta}\left(\frac{\partial \eta}{\partial t} \frac{c_b E_b f_{bk} r_b}{J} + \frac{q_{b\eta k}}{J} \right) = 0$$

$$\begin{cases} F_{bk} = f_{d1k}, & \partial z_b / \partial t \leq 0 \\ F_{bk} = f_{bk}, & \partial z_b / \partial t \geq 0 \end{cases} \tag{10}$$

$$\frac{\partial}{\partial t}\left(\frac{E_{d1} f_{d1k}}{J} \right) - F_{dk} \frac{\partial}{\partial t}\left(\frac{E_{d1}}{J} \right) = 0$$

$$\begin{cases} F_{dk} = f_{d1k}, & \partial z_b / \partial t \leq 0 \\ F_{dk} = f_{bk}, & \partial z_b / \partial t \geq 0 \end{cases} \tag{11}$$

In the formulae above, f_{bk} is the concentration of bed load of size class k in the bed load layer, f_{dmk} is the sediment concentration of size class k in the mth bed layer, c_b is the depth-averaged concentration of bed load. E_{be} is the equilibrium bed load layer thickness; it is estimated by the following equation [3]:

$$\frac{E_{be}}{d_m} = \frac{1}{c_b \cos\theta\left(\tan\phi - \tan\theta\right)} \tau_{*m} \tag{12}$$

where d_m is the mean diameter of bed load, ϕ is the angle of repose, and τ_{*m} is the non-dimensional shear stress of mean diameter. E_{sd} is the sediment layer thickness on cohesive sediment bed. E_b is the bed load layer thickness, $q_{b\xi k}$ and $q_{b\eta k}$ are the bed load of size class k in ξ and η directions, respectively, q_{bxk} and q_{byk} are the bed load of size class k in x and y directions, respectively as follows [1, 2 and 6].

$$q_{bxk} = q_{bk} \cos\beta_k \tag{13}$$

$$q_{byk} = q_{bk} \sin\beta_k \tag{14}$$

$$q_{bk} = 17 \frac{\rho u_{*e}^3}{(\rho_s - \rho) g} \left(1 - \sqrt{K_c} \frac{u_{*ck}}{u_*}\right) \left(1 - K_c \frac{u_{*ck}^2}{u_*^2}\right) f_{bk} \tag{15}$$

Therein, ρ_s is the sediment density, u_{*e} is the effective shear velocity, the non-dimensional critical friction velocity of size class k is evaluated as follows [1].

$$u_{*ck}^2 = u_{*cm}^2 \left[\frac{\log_{10} 19}{\log_{10}(19 d_k / d_m)} \right]^2 \frac{d_k}{d_m} \quad d_k / d_m \geq 0.4 \tag{16-1}$$

$$u_{*ck}^2 = 0.85 u_{*cm}^2 \qquad d_k / d_m \leq 0.4 \tag{16-2}$$

Iwagaki's formula [5] which is formulated for uniform bed material is used for evaluating u_{*cm}. K_c is a correction factor due to the influence of bed inclination on sediment motion.

$$K_c = 1 + \frac{1}{\mu_s} \left[\left(\frac{\rho}{\rho_s - \rho} + 1 \right) \cos\alpha \tan\theta_x + \sin\alpha \tan\theta_y \right] \tag{17}$$

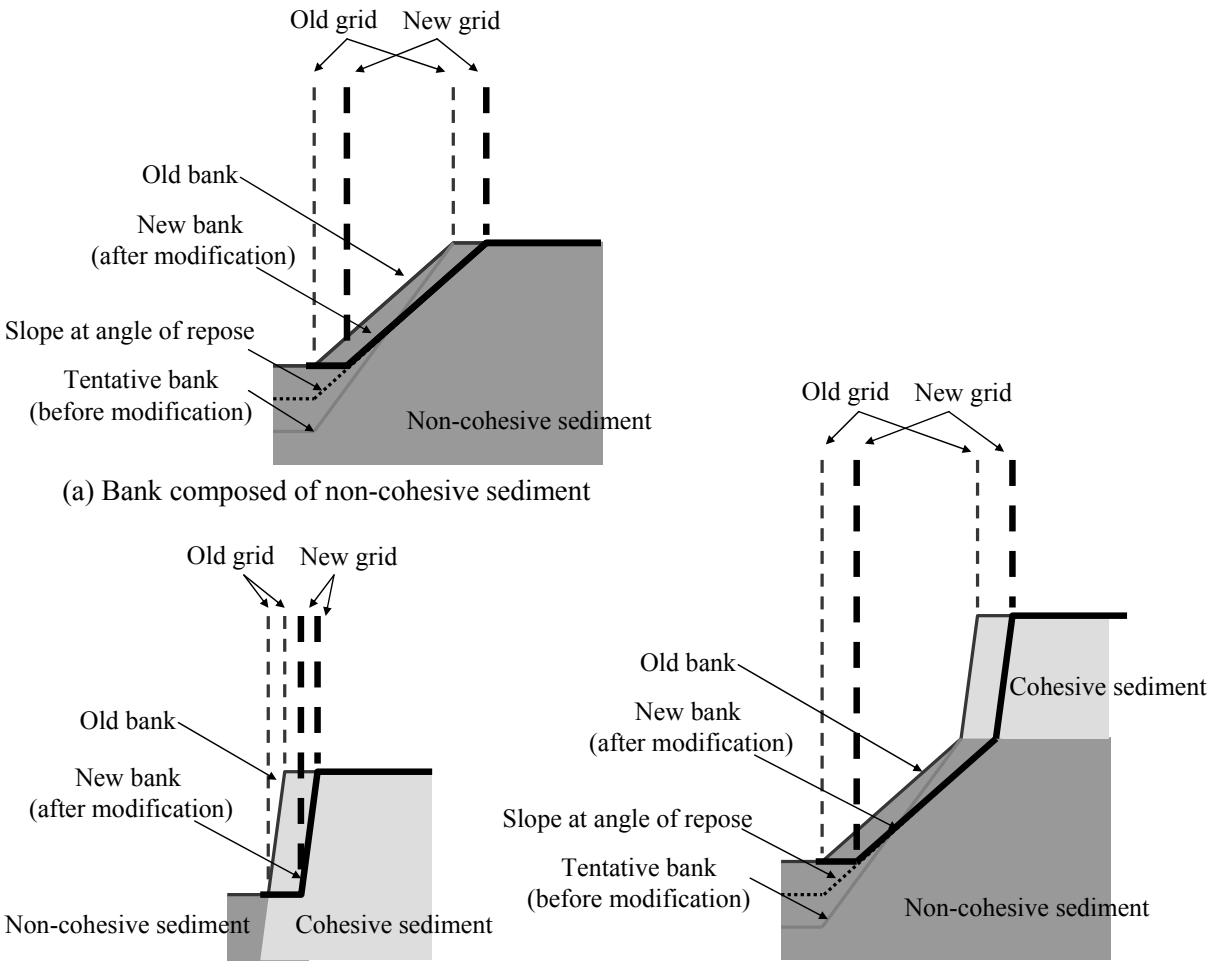

(a) Bank composed of non-cohesive sediment

(b) Bank composed of cohesive sediment

(c) Bank composed of cohesive and non-cohesive sediment

Figure 4 conceptual diagram of bank erosion model

where α is the angle of deviation of near-bed flow from the *x* direction as follows.

$$\alpha = \arctan\left(\frac{v_b}{u_b}\right) \tag{18}$$

μ_s is the coefficient of static friction. θ_x and θ_y are bed inclinations in the *x* and *y* directions, respectively. These inclinations are evaluated as follows,

$$\theta_x = \arctan\left(\frac{\partial \xi}{\partial x}\frac{\partial z_b}{\partial \xi} + \frac{\partial \eta}{\partial x}\frac{\partial z_b}{\partial \eta}\right) \tag{19}$$

$$\theta_y = \arctan\left(\frac{\partial \xi}{\partial y}\frac{\partial z_b}{\partial \xi} + \frac{\partial \eta}{\partial y}\frac{\partial z_b}{\partial \eta}\right) \tag{20}$$

Hence, the local bed slope along direction of bed load of sediment mean diameter (θ) is obtained as follows.

$$\sin\theta = \cos\beta_m \sin\theta_x + \sin\beta_m \sin\theta_y \tag{21}$$

where β_m is the deviation angle of bed load of mean diameter to the *x* direction. The deviation angle of bed load of size class *k* to the *x* direction (β_k), which depends on the flow near bed and inclination of the bed, is calculated by the following relation.

$$\tan\beta_k = \frac{\sin\alpha - \Pi\Theta_y\left(\frac{u_{*ck}^2}{u_*^2}\right)\tan\theta_y}{\cos\alpha - \Pi\Theta_x\left(\frac{u_{*ck}^2}{u_*^2}\right)\tan\theta_x} \tag{22}$$

$$\Pi = K_{ld} + 1/\mu_s \tag{23}$$

$$\Theta_y = \frac{1}{1+\tan^2\theta_x + \tan^2\theta_y} \tag{24}$$

$$\Theta_x = \Theta_y + \frac{\rho}{\rho_s - \rho}\cos^2\theta_x \tag{25}$$

Evolution of bed elevation is estimated by means of following formulae.

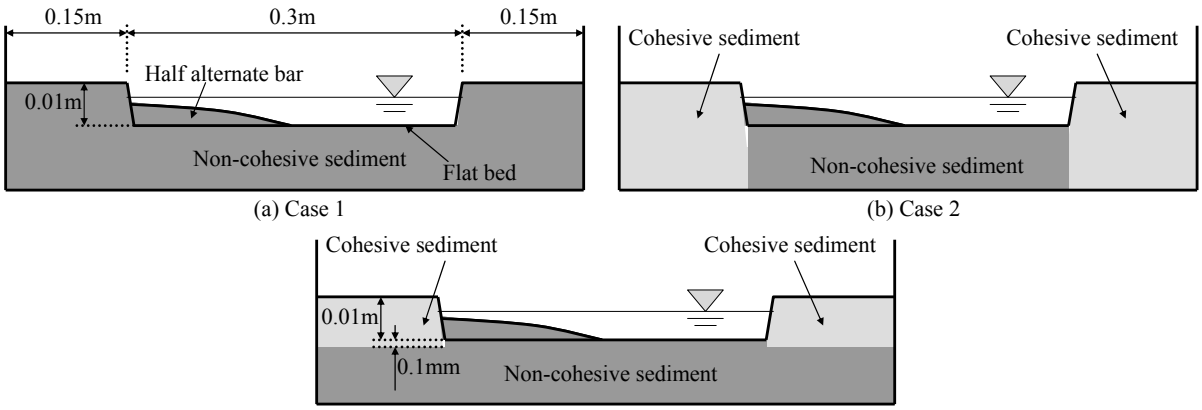

(a) Case 1 (b) Case 2

(c) Case 3

Figure 5 Initial cross-sectional shapes of channels

$$\frac{\partial}{\partial t}\left(\frac{c_b E_b}{J}\right)+(1-\lambda)\frac{\partial}{\partial t}\left(\frac{z_b}{J}\right) + \frac{\partial}{\partial \xi}\left(\frac{\partial \xi}{\partial t}\frac{c_b E_b}{J}+\sum_{k=1}^{n}\frac{q_{b\xi k}}{J}\right) + \frac{\partial}{\partial \eta}\left(\frac{\partial \eta}{\partial t}\frac{c_b E_b}{J}+\sum_{k=1}^{n}\frac{q_{b\eta k}}{J}\right)=0 \tag{26}$$

In them, n represents the number of the size class of sediment.

3. 2. Bank erosion model

Figure 4 shows the conceptual diagram of bank erosion model. When bank is composed of non-cohesive material and bed near the bank is eroded, the bank line is shifted with keeping the slope geometry at the angle of repose. The location of numerical grids will be shifted as shown in Figure 1(a). When bank is composed of cohesive material, bank line is shifted at the speed of erosion velocity of the cohesive material. The erosion velocity of cohesive sediment (V_e) is estimated as follows [8].

$$V_e = \alpha_c R_{wc}^{2.5} u_*^3 \tag{27}$$

where, α_c is the coefficient related on kinds of cohesive sediment, R_{wc} is the water content rate. When bank material is composed of cohesive material, the bed degradation near the bank does not affect on the bank erosion. Here, for simplicity, it is assumed that the eroded cohesive material is transported to downstream area immediately and does not affect on bed deformation. When bank material is composed of both non-cohesive material and cohesive material, the treatment of the bank erosion becomes more complex. In the present research, the bank which has upper bank layer composed of cohesive material and lower bank layer with non-cohesive material, as shown in Figure 4 (c), is treated. When the bed level near the bank is higher than the bottom level of cohesive material layer, the entire bank is composed of cohesive material. Hence, the bank erosion process is the same as Figure 4 (b). When the bed level near the bank is lower than the bottom level of cohesive material layer, the lower part of bank is composed of non-cohesive material. Hence, the bank erosion process is the same as Figure 4 (c). The bank composed of non-cohesive material forms the slope at the angle of repose. Hence, the cohesive layer will be overhanged because of the erosion of lower layer composed of non-cohesive material and it is assumed here that the overhanged cohesive material is collapsed immediately.

3. 3. Hydraulic conditions

The simulated domain is a 7.5 m long rectangular and straight open channel. The width of the simulated domain is 0.6m. At the center of the simulated domain, a channel which has 0.3m wide and 1cm depth is made as shown in Figure 5. Periodical alternate bar with 1.8m wavelength and 0.75cm wave height is formed on the initial bed geometry in the channel. Here, the troughs of the alternate bars are made flat in order to clarify the effect of bed degradation on bank erosion. The initial longitudinal bed slope is 1/70. The bed materials are treated as non-uniform sediment with the mean diameter of 0.43 mm. Water discharge is 0.75l/s and normal flow depth is about 0.67cm. The hydraulic condition in the channel is located in the

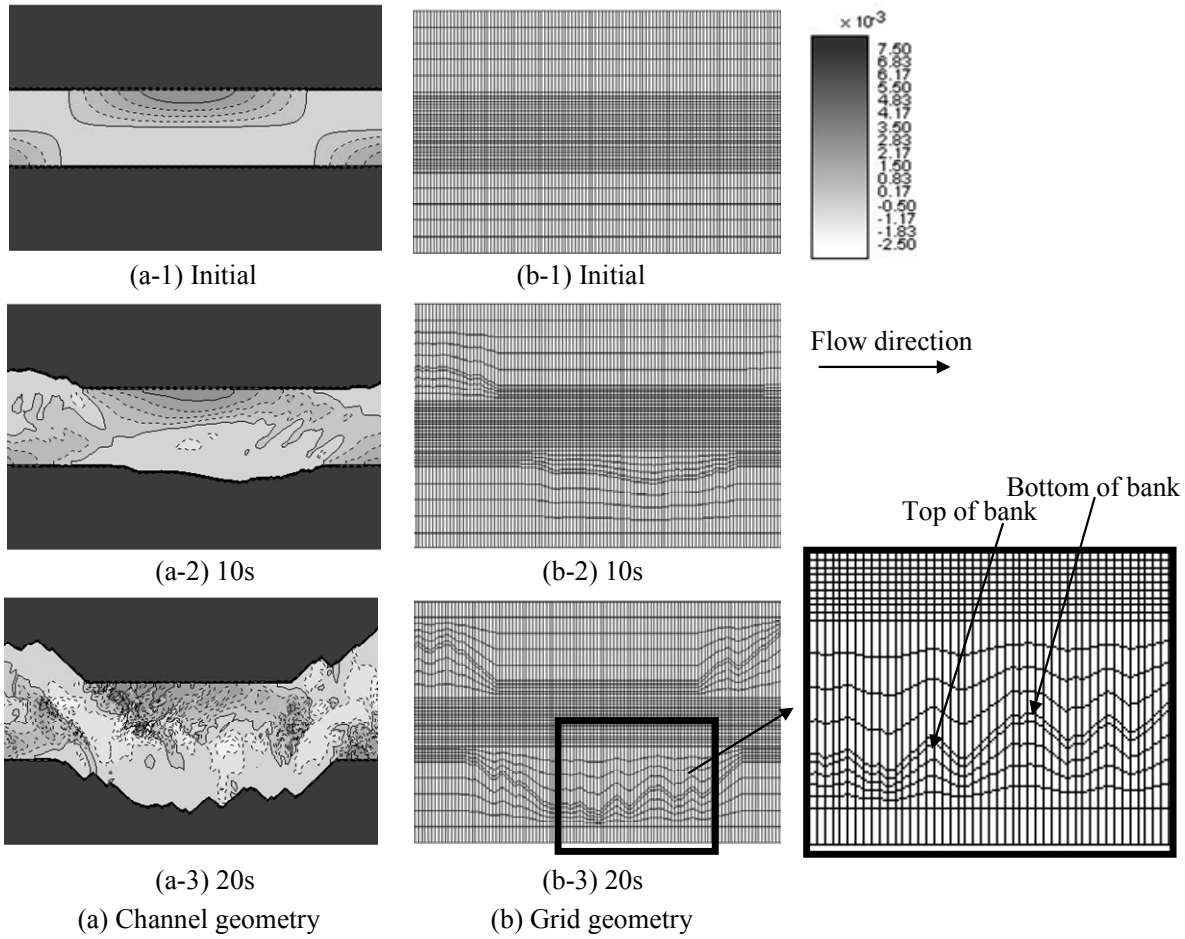

(a-1) Initial (b-1) Initial

(a-2) 10s (b-2) 10s

(a-3) 20s (b-3) 20s

(a) Channel geometry (b) Grid geometry

Figure 6 Temporal changes of channel geometry and numerical grid geometry

formative conditions of alternate bars. In Case 1, both the bed and the bank material are treated as non-cohesive material. In Case 2, the bed material is non-cohesive material, but bank material is cohesive material. In Case 3, the upper bank material with 1.01cm thickness is cohesive material and the lower bank material is non-cohesive material. Hence, at the initial condition, entire bank is composed of cohesive material in Case 3, but after bed is eroded in 0.1mm depth, the non-cohesive layer exposed at the bottom of the bank.

4. Results and discussio

Figure 6 shows the temporal changes of channel geometry and numerical grid geometry. Grid geometry around banks is transformed with the shift of bank lines. Here, the transverse distance of grids between bottom of bank and top of bank is kept constant with time to keep the accuracy to estimate the angle of repose constant. If the distance of grids between bottom of bank and top of bank becomes wider with widening of river width, the accuracy to estimate the angle of repose decreases with time. As a result, the bank erosion velocity becomes slower because of the rough grids and it is very difficult to discuss the bank erosion process.

Figure 7 shows the temporal change of channel geometry in Cases 1, 2, and 3. At the initial stages, horizontal shapes of all channel geometries are straight. After 5s, bank is started to be eroded in Case 1 (non-cohesive). Banks of both Case 2 (cohesive) and Case 3 (non-cohesive and cohesive) are also eroded at 5s. However, the erosion velocity of cohesive material is slower than the bank erosion velocity with non-cohesive material. Hence the shifts of bank in Cases 2 and 3 are invisible at 5s. Here, in Case 3, the bottom level of cohesive material is still lower than the bed level near the bank. After 10s, bank is shifted more in Case 1. The shift of bank in Case 2 is still invisible at 10s. In Case 3, the shift of bank becomes visible at 10s.

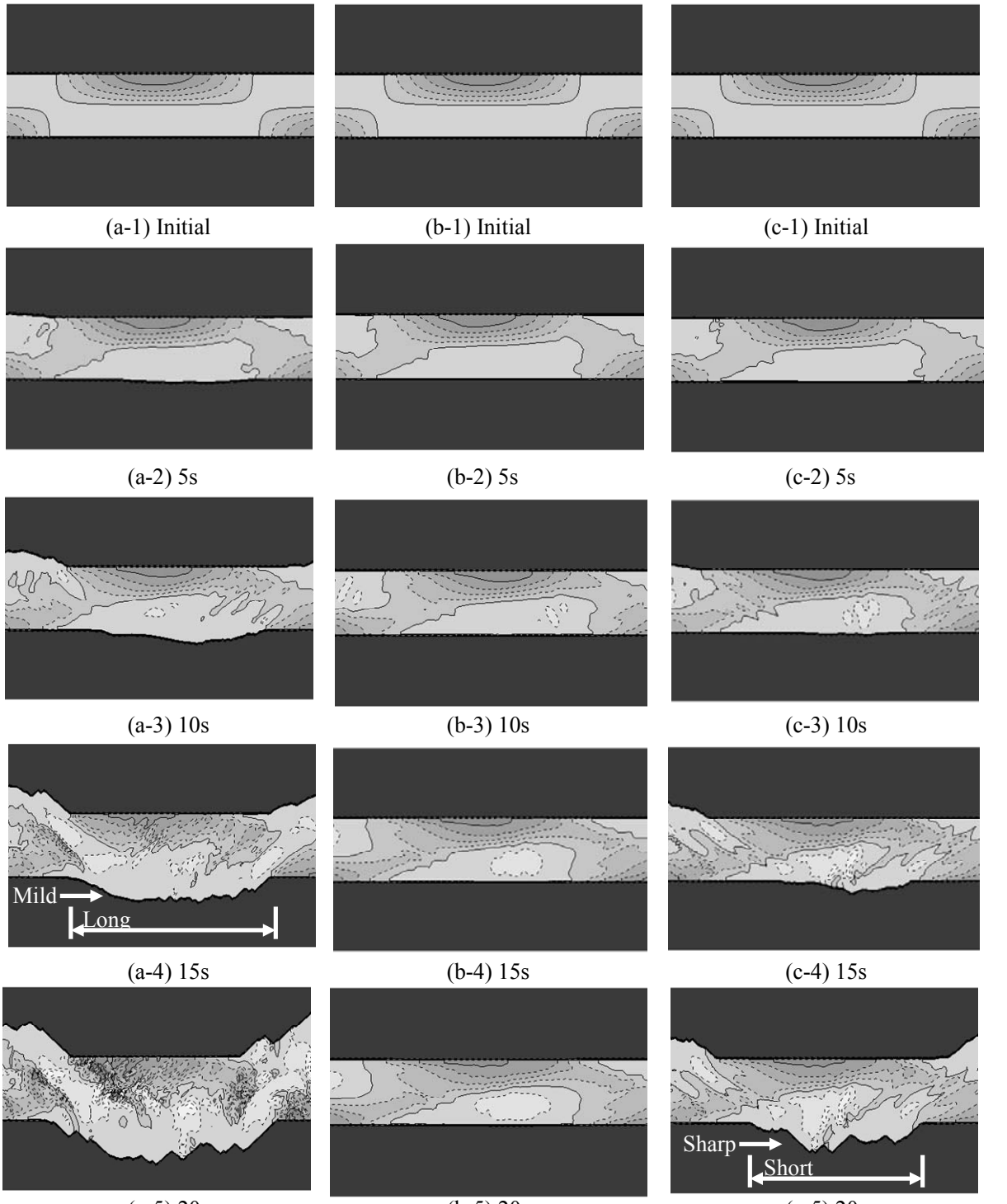

Figure 7 Temporal changes of channel geometry

This means that the bed level near the bank becomes higher than the bottom level of cohesive material at some areas. After 15s, bank is shifted more in Case 1. In Case 3, bank erosion velocity increased rapidly. Here, apparently, the bank erosion velocity depends on the landslide of non-cohesive sediment to keep the angle of repose. These results indicate that in case that upper and lower bank materials are composed of cohesive material and non-cohesive material, respectively, the bank erosion rate increases rapidly. The rapid temporal change of bank erosion velocity tends to cause severe disaster due to bank erosion, because residents near the bank cannot predict such a rapid

change of erosion velocity. In Case 2, the bed near bank is decreased with time, but the bank erosion rate does not increase with time, because the entire bank is composed of cohesive material. After 20s, banks are shifted more with time in Cases 1 and 3. Here, shape of bank line in Case 3 at 20s is compared to that in Case 1 at 15s. The maximum transverse distance of bank erosion in Case 1 at 15s is the same as that in Case 3 at 20s. However, the shapes of the bank lines are different. The longitudinal length of bank erosion area in Case 1 is longer than that in Case 3. Furthermore, the shape of the bank line in Case 1 is milder than that in Case 3. The temporal change of longitudinal distribution of bed along bottom of bank causes the difference. As mentioned above, the erosion velocity of cohesive material is slower than the erosion velocity of bank with non-cohesive material. If bed near bank is eroded and lower layer with non-cohesive material is exposed to flow locally, the bank is only eroded faster. Hence, the horizontal shape of bank lines in Case 3 is sharp and local curvature of bank lines becomes small.

5. Conclusion

In this study, mathematical model of bank erosion process for banks with both the cohesive and non-cohesive layers is developed. Furthermore, the model is installed into the horizontal two dimensional channel deformation model. The results indicate that the horizontal shift speed of banks changes with time very much. When the bottom layer with non-cohesive material is not exposed to the flow, the speed of bank erosion is very slow. However, when bed near the bank is eroded with time and bottom layer starts to be exposed to flow, the bank erosion rate increases rapidly and it is considered that a severe disaster is caused. The calculated horizontal shape of bank lines with both cohesive and non-cohesive materials is not so smooth and local curvature of bank lines becomes small.

Acknowledgements

This work is funded by Grant-in-Aid for Scientific Research (A) (Representative: Yasuyuki Shimizu), Grant-in-Aid for Scientific Research for young researchers (B) (Representative: Hiroshi Takebayashi), RIC Research Fund (Representative: Hiroshi Takebayashi), Research Fund from Foundation of River & Watershed Environment Management (Representative: Hiroshi Takebayashi), STC Research Fund (Representative: Hiroshi Takebayashi), and GCOE Global Center for Education and Research on Human Security Engineering for Asian Megacities (Representative: Yuzuru Matsuoka).

References

[1] Ashida, K. and Michiue, M. Study on hydraulic resistance and bed-load transport rate in alluvial streams, *Proc. of JSCE*, No. 206, pp.59-69, 1972.

[2] B. Y. Liu Study on Sediment Transport and Bed Evolution in Compound Channels. *Thesis presented to Kyoto University*, 1991.

[3] Egashira, S. and Ashida, K. Unified view of the mechanics of debris flow and bed-load, *Advances in Micromechanics of Granular Materials*, (Edited by H.H.Shen et al.) Elsevier, pp. 391-400, 1992.

[4] Engelund, F. Flow and bed topography in channel bends. *Jour. of Hy. Div. ASCE*, Vol. 100, No. HY11, 1974.

[5] Iwagaki, Y. Hydrodynamic study on critical shear stress. *Proc. of JSCE*, No. 41, pp. 1-21, 1956.

[6] Kovacs, A. and Parker, G. A new vectorial bedload formulation and its application to the time evolution of straight river channels. *J. Fluid Mech. Vol.* 267, pp. 153-183, 1994.

[7] Nagata, N. Numerical analysis of the 2-dimensional unsteady flow using a generalized coordinate system, *The lecture collection on the computer use in hydraulic engineering, the Japan Society of Civil Engineers*, pp. 51 – 76, 1999.

[8] Sekine, M., Nishimori, K., Fujio, K. and Katagiri, Y. On erosion process of cohesive sediment and erosion rate formula, *Annual Journal of Hy. Eng. JSCE*, Vol. 47, pp. 541-546, 2003.

[9] Shimizu,Y. and Itakura,T. Calculation of flow

and bed deformation with a general non-orthogonal coordinate system, *Proc. of XXIV IAHR Congress*, Madrid, Spain, C-2, pp.41-48, 1991.
[10] Takebayashi, H. River Configuration in Middle-Lower Reach of River Basin, *Journal of Japan Society of Fluid Mechanics*, Vol. 24, pp. 27-36, 2005.
[11] Takebayashi, H., Egashira, S. and Okabe, T. Braided streams formed on beds with non-uniform sediment, *Proc. 3nd IAHR Symposium on River, Coastal and Estuarine Morphodynamics*, pp.787-798, 2003.

粘着性土と非粘着性土が混在した河岸の浸食解析モデル

竹林洋史・藤田正治・プジハルサント

要　旨

実河川では，粘着性土と非粘着性土が互層になっている河岸がよく見られる（例えば，インドネシア・カリマンタン島のセサヤップ川等）。本研究では，河岸の上層が粘着性土，下層が非粘着性土で構成された河岸の浸食過程の数理モデルを構築した。さらに，構築した河岸浸食モデルを移動一般座標系の平面二次元河床変動解析モデルに導入し，解析を試みた。その結果，粘着性土と非粘着性土が混在した河岸では，河岸の浸食速度を時間的に大きく変化することが明らかとなった。つまり，河床の洗掘が十分でなく，下層の非粘着性土が流れに露出していないときは，河岸の浸食速度は非常に遅くなる。一方，河床の洗掘が進み，非粘着性土が流れに露出し始めると，河岸浸食速度は急激に速くなる。このような浸食速度の急激な変化は，河岸の質に関する情報が無い場合は予測が難しく，河川近傍の住民の河岸浸食対策が遅れがちになり，大きな災害を引き起こす可能性が高い。

キーワード：河岸浸食，粘着性土，数値解析，移動一般座標系